Applied Catalysis B: Environmental 117–118 (2012) 204–211

Contents lists available at SciVerse ScienceDirect

Applied Catalysis B: Environmental

journal homepage: www.elsevier.com/locate/apcatb

Methanol-tolerant Pd nanocubes for catalyzing oxygen reduction reaction in H_2SO_4 electrolyte

Chien-Liang Lee*, Hsueh-Ping Chiou

Department of Chemical and Materials Engineering, National Kaohsiung University of Applied Sciences, Kaohsiung 807, Taiwan

ARTICLE INFO

Article history:
Received 29 November 2011
Received in revised form 5 January 2012
Accepted 10 January 2012
Available online 18 January 2012

Keywords:
Pt nanoparticles
Cathodic catalysts
Crystal face

ABSTRACT

New methanol-tolerant catalysts in the form of 27 nm, 48 nm, and 63 nm palladium nanocubes enclosed by {1 0 0} facets were successfully used for the oxygen reduction reaction (ORR) in a 0.5 M $H_2SO_{4(aq)}$ solution. Based on X-ray photoelectron spectroscopy and high resolution transmission electron microscopy analyses, the surface of the smallest Pd nanocubes was easily oxidized to PdO. The data provided by the analysis of a mass-transfer-corrected Tafel curve in a free methanol electrolyte showed that the specific activities of the 27 nm, 48 nm, and 63 nm Pd nanocubes at 0.65 V (vs. Ag/AgCl) in terms of the kinetic current density (j_k) were 11.51×10^{-2} mA cm^{-2}, 12.32×10^{-2} mA cm^{-2}, and 10.06×10^{-2} mA cm^{-2}, respectively. In contrast, Pd and Pt nanoparticles featured specific activities of 3.7×10^{-2} mA cm^{-2} and 13.2×10^{-2} mA cm^{-2}, respectively. Further Tafel analyses conducted using a rotating ring-disk electrode in a methanol electrolyte showed that the j_ks of the 27 nm, 48 nm, and 63 nm Pd nanocubes at 0.65 V (vs. Ag/AgCl) were 14.87×10^{-2} mA cm^{-2}, 16.55×10^{-2} mA cm^{-2}, and 12.98×10^{-2} mA cm^{-2}, respectively. The nanocubes have a high activity toward the ORR; the greatest j_k was occurred on the 48 nm nanocube even larger than 5.65×10^{-2} mA cm^{-2}, the j_k of the Pd nanoparticles in the methanol electrolyte, where Pt nanoparticles effected methanol oxidation in preference to the ORR. Despite working in methanol-tolerant solutions, the prepared 48 nm Pd nanocubes exhibited high electroactivity.

1. Introduction

The manipulation of the shape of nanoparticles enclosed by specific crystal facets is currently an interesting strategy in electrocatalysis [1,2] that is applied for green energy in fuel cells. Recently, cubic Pt nanoparticles with {1 0 0} facets were found to have a greater activity compared to polyhedral Pt electrocatalysts dominated by (1 1 1) planes toward the oxygen reduction reaction (ORR) [3], which is the limiting reaction for acidic fuel cells. This shape-dependent ORR activity was ascribed to the minor adsorption power of sulfate ions on the crystallographic (1 0 0) facets when the nanocubes were used as electrocatalysts in a H_2SO_4 electrolyte. The adsorption of the sulfate ions is due to symmetry matching binding between the three O atoms in the sulfate ion and Pt atoms on the (1 1 1) surface. This increased adsorption can inhibit ORR kinetics on Pt(1 1 1). The activity of Pt nanocubes on carbon nanotubes was further tested and concluded to be higher than that of Pt/C [4], which is a commercial ORR electrocatalyst. The desirable properties of nanocubes were confirmed when gold nanocubes also showed unique activity toward the ORR in a 0.1 M NaOH electrolyte [5]. The ORR proceeded via a fast 4-electron pathway on the surface of the (1 0 0) facets of these Au nanocubes, unlike a well-known and slower 2-electron ORR that occurs on bulk Au(1 1 1) [6]. For Pt, Au, and Pd nanoparticles, which are face-centered cubic (fcc) crystal materials, the surface energies of the low-index crystallographic planes are in the order (1 0 0) plane > (1 1 1) plane [7]. This could be the underlying reason for the unique properties of electrocatalysts domained by (1 0 0) planes toward ORRs.

Among noble nanoparticles, palladium is a potential catalyst to replace platinum, which is easily poisoned by alcohols in the ORR [8]. Some studies have revealed that Pd-based electrocatalysts such as Pd–Fe [9], Pd–Co [10–13], Pd–W [14], and Pd–Pt [15–17] exhibit methanol-tolerant properties and maintain high activity toward ORR, which is important if alcohol crossover occurs in direct alcohol fuel cells. Recently, we also demonstrated the feasibility of Ag–Pd [18] and Pd–Pt [19] nanoparticles as ORR catalysts in NaOH and H_2SO_4 electrolytes, respectively, that contain methanol. Furthermore, Kondo et al. [20] successfully demonstrated the order Pd(1 1 0) < Pd(1 1 1) < Pd(1 0 0) with regard to the activity toward ORRs in acidic mediums and further concluded that the specific activity of Pd(1 0 0) is three times greater than that of Pt(1 1 0), which is the Pt plane with the highest activity. Herein, different sizes of Pd nanocubes enclosed by (1 0 0) planes were prepared as

* Corresponding author at: No. 415, Chien Kung Rd., Kaohsiung 807, Taiwan. Tel.: +886 7 3814526 5131; fax: +886 7 3830674.
E-mail addresses: cl_lee@url.com.tw, cl_lee@kuas.edu.tw (C.-L. Lee).

0926-3373/$ – see front matter © 2012 Elsevier B.V. All rights reserved.
doi:10.1016/j.apcatb.2012.01.012

new methanol-tolerant ORR electrocatalysts in a 0.5 M $H_2SO_{4(aq)}$ electrolyte. Subsequently, as supported by electrochemical analyses, a fair comparison in terms of the specific and mass activities was made between the various Pd nanocubes, Pd nanoparticles, and Pt nanoparticles.

2. Experimental

2.1. Preparation of nanocubes

The method to synthesize 27 nm, 48 nm, and 63 nm Pd nanocubes, which was originally used for the preparation of 48 nm and 63 nm Pd nanocubes, is based on the study of Xu [21] and is as follows: initially, 500 μL of a 0.01 M H_2PdCl_4 aqueous solution was added to 10 mL of a 1.25×10^{-2} M hexadecyltrimethyl ammonium bromide (C_{16}TAB) aqueous solution at a fixed temperature of 95 °C. Then, 80 μL of a 0.1 M vitamin C solution was gradually added to the mixture with stirring. A dark brown 27 nm Pd nanocube solution was thus obtained. Afterwards, 125 μL of 0.01 M H_2PdCl_4 was added to 5 mL of a 0.05 M C_{16}TAB aqueous solution. Further, 25 μL of 0.1 M vitamin C and 400 μL of the prepared 27 nm Pd nanocube solution, used as a seed solution, were slowly added to the C_{16}TAB aqueous solution at 40 °C. Pd nanocubes that were 48 nm in edge length were thus prepared after reacting for 14 h. Likewise, the 63 nm Pd nanocubes were obtained by changing the amount of seed solution from 400 μL to 80 μL in the synthetic pathway.

For a fair comparison of ORR activity, Pd and Pt nanoparticles were prepared. For the synthesis of Pd nanoparticles, 500 μL of a 0.01 M H_2PdCl_4 aqueous solution was added to 10 mL of a 1.25×10^{-2} M $C_{16}TAB_{(aq)}$ solution at 95 °C. Then, 5 μL of a 16 M N_2H_4 solution was added dropwise to reduce the Pd nanoparticles. Based on the same method and using H_2PtCl_6 in place of H_2PdCl_4, Pt nanoparticles were synthesized.

2.2. Analyses of materials

The characteristic size, shape, and structure of the prepared nanocubes in solution, which were dipped in both a copper grid and a smooth silicon substrate and dried naturally, were observed under a high-resolution transmission electron microscope (HRTEM; JEOL JEM-3000F) and a field emission scanning electron microscope (FE-SEM; Hitachi S4800-I). The X-ray diffraction (XRD) patterns and the X-ray photoelectron spectra (XPS) of the prepared nanocubes were obtained using XRD spectroscopy (Shimadzu XD-3A, Cu anode) and XPS spectroscopy (Kratos Axis Ultra DLD), respectively.

2.3. Electrochemical analyses

The electrochemical activity of the Pd nanocubes prepared for use in cyclic voltammetry (CV) or linear scanned voltammetry (LSV) experiments was evaluated by performing a rotating ring disk electrode (RRDE) measurement. First, a solution containing 78 μg of Pd catalyst and 3 μL of 5% Nafion were dropped onto a 0.196 cm^2 GCE disk, which was then heated to 60 °C to evaporate the water. An RRDE measurement was carried out using a combination of an RRDE system (AFMSRCE, Pine Co., Ltd.) and a bipotentiostat (CHI 727D). A rotating glassy carbon disk-platinum ring electrode (ring area: 0.11 cm^2) was used as the working electrode. In addition, a Pt counter electrode and an Ag/AgCl (3 M KCl) reference electrode were used for measurements in N_2- or O_2-saturated 0.5 M $H_2SO_{4(aq)}$ solutions with or without 0.5 M methanol. For the LSV measurements, the ring potential was maintained at 1.2 V to oxidize the H_2O_2 produced by the O_2 reduction at the disk electrode. The collection factor (N) was 0.27.

3. Results and discussion

Fig. 1A–C shows TEM images of the prepared seeds and the two larger Pd nanocubes in low scales, respectively. As evident in Fig. 1A, the cubic nanoparticles were formed in a high yield. Based on the growth on the seed structure, as seen in Fig. 1A, the sizes of the Pd nanocubes shown in Fig. 1B and C increased while maintaining a uniform cubic shape. With a decrease in the amount of seed added, the edge length of the nanocubes increased. The statistics on the edge lengths of these nanocubes, as captured by TEM images, are presented in Fig. 2. The mean edge length of the seed nanocubes was 27 nm. When 400 μL of the seed nanocube solution was added to the growth solution containing H_2PdCl_4, the mean edge length of nanocubes increased to 48 nm, while the mean edge length was 63 nm if 80 μL of the seed nanocube solution was used. This shows that the nanocubes used as methanol-tolerant ORR electrocatalysts in this study were of different sizes. Typically, Pt [22] or Pt-based alloy [23] nanocubes are enclosed by (1 0 0) planes. Fig. 1D depicts an electron diffraction pattern obtained by using an electron beam for a single nanocube of the size shown in Fig. 1C. This single-crystal-like pattern indicates that the cubic nanoparticle is surrounded by {1 0 0} planes. In the two TEM images shown in Fig. 1B and C, some domino-stacked nanocubes are observed and the morphologies of the lower nanocubes are evident. This indicates that the prepared nanoparticles could be square-like nanoplates or nanosheets. Fig. 3A–C shows the FE-SEM images of the 27 nm, 48 nm, and 63 nm square-like nanoparticles, respectively, spreading out along a smooth silicon substrate. High yields of the cubic nanoparticles are observed, which is particularly clear for the rolling larger nanocubes in Fig. 3B and C. This measured result eliminates the possibility of nanoplates.

To study the composition of the prepared nanocubes, XRD measurements were performed to detect spreading nanocubes, as seen in the FE-SEM images of Fig. 3. Fig. 4 shows the XRD pattern of the synthesized 27 nm, 48 nm, and 63 nm nanocubes. For the 27 nm Pd nanocubes, characteristic diffraction peaks are observed at 2θ values of 40.04°, 46.51°, 68.04°, 82.05°, 86.52°, and 104.67°, which were assigned to Pd(1 1 1), Pd(2 0 0), Pd(2 2 0), Pd(3 1 1), Pd(2 2 2), and Pd(4 0 0), respectively. These results, which are similar to those of the 48 and 63 nm Pd nanocubes, are consistent with the Pd standard spectrum (JCPDS 65-2867), thus supporting the conclusion that the bright nanocubes in Fig. 3 are composed of metallic palladium. To further investigate the chemical state on the surface of these Pd nanocubes, XPS measurements were carried out. It should be noted that the surface of small Pd nanocubes can be easily oxidized from metallic Pd to PdO. Fig. 5 shows the XPS spectrum of Pd for the 27 nm, 48 nm, and 63 nm Pd nanocubes. The locations of all the measured XPS peaks are summarized in Table 1. For the 63 nm Pd nanocube, two peaks, Pd $3d_{3/2}$ and Pd $3d_{5/2}$, were detected at 340.65 eV and 335.36 eV, respectively. These peaks were close to the electron binding energies of metallic Pd found in the handbook at 340.5 eV and 335.2 eV [24]. Simultaneously, another pair of peaks, Pd $3d_{3/2}$ and Pd $3d_{5/2}$, located at 338.32 eV and 336.16 eV, respectively, were obtained. This measured peak pair is similar to the XPS spectrum of Pd^{2+} [25] in which the Pd $3d_{3/2}$ peak is

Table 1
The summarized $Pd_{3/2}$ and Pd $_{5/2}$ locations of XPS spectra of different Pd nanocubes.

Pd nanocube	Pd $3d_{3/2}$			Pd $3d_{5/2}$		
	Pd^0	PdO	Pd^{2+}	Pd^0	PdO	Pd^{2+}
27 nm	340.66	341.77		335.41	336.66	
48 nm	340.52		338.4	335.23		333.2
63 nm	340.65		338.32	335.36		333.16
Refs. [24,25]	340.52	342.3	338.23	335.26	336.3	332.97

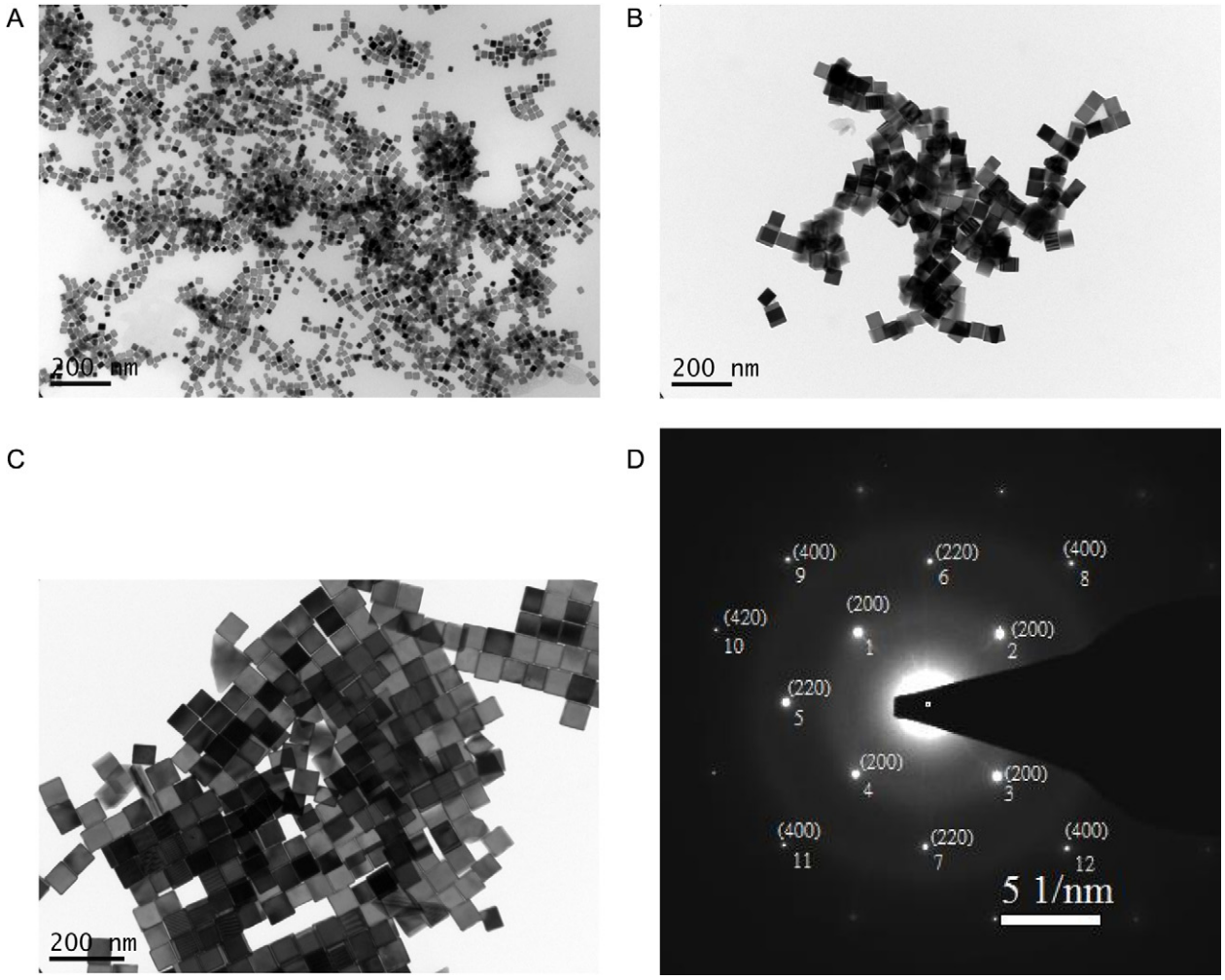

Fig. 1. TEM images and diffraction pattern of Pd nanocubes: (A) 27 nm nanocubes; (B) 48 nm nanocubes; (C) 63 nm nanocubes; (D) diffraction pattern of 63 nm Pd nanocube.

located at 338.23 eV and the Pd $3d_{5/2}$ peak is located at 332.97 eV. This indicates that excess Pd^{2+} was adsorbed on the Pd nanocubes during the synthetic pathway. Similar results for the 48 nm Pd nanocubes can be found in the XPS spectrum shown in Fig. 5 and summarized in Table 1. In contrast to the XPS spectra of the 48 and 63 nm nanocubes, the XPS spectrum of the 27 nm nanocubes show unexpected XPS peaks corresponding to Pd $3d_{3/2}$ and Pd $3d_{5/2}$ at 341.77 eV and 336.66 eV, respectively, which indicate the formation of PdO on the nanocube surface. The correlation of these Pd $3d_{3/2}$ and Pd $3d_{5/2}$ locations with PdO was confirmed by comparing them to an XPS study of a Pd–O electrode [26]. Additional supporting data from the HR-TEM observations, as shown in the inset of Fig. 5, indicate a uniform gray shell coated on the metallic core of the 27 nm Pd nanocubes. The XPS spectrum and the HR-TEM image indicate that the surface of smaller Pd nanocubes (~27 nm) and nanocube powders easily produces a PdO layer when exposed to the atmosphere. In other words, the (1 0 0) surface of the 27 nm Pd nanocube is more reactive toward O_2 than those of the 48 nm and 63 nm Pd nanocubes.

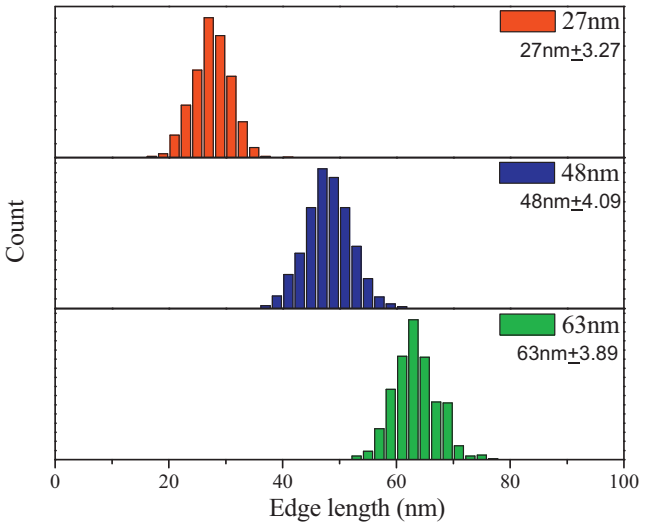

Fig. 2. Bar plots for the statistic in the size of different Pd nanocubes.

The catalytic potential of these nanocubes toward acidic ORRs was then examined. Their electrochemical properties were initially measured by CV. Fig. 6A shows a comparison of the CV curves obtained by measuring the electrochemical responses of the Pd nanocubes in 0.5 M $H_2SO_{4(aq)}$ solutions under an N_2 atmosphere. For the 48 nm Pd nanocubes, the electrochemical response from 0.1 V to −0.2 V (vs. Ag/AgCl) is associated with the hydrogen adsorption/desorption region on the Pd surface, while the long and narrow region from 0.5 V to 0.1 V is attributed to the contribution of the electric double-layer. The peak located at 0.55 V corresponds to the reduction of PdO produced via cathodic CV scanning at a scan rate of 50 mV s^{-1}. The shape of this CV curve is similar to that of Pd nanocubes bound with poly(vinylpyrrolidone) [27]. It should be

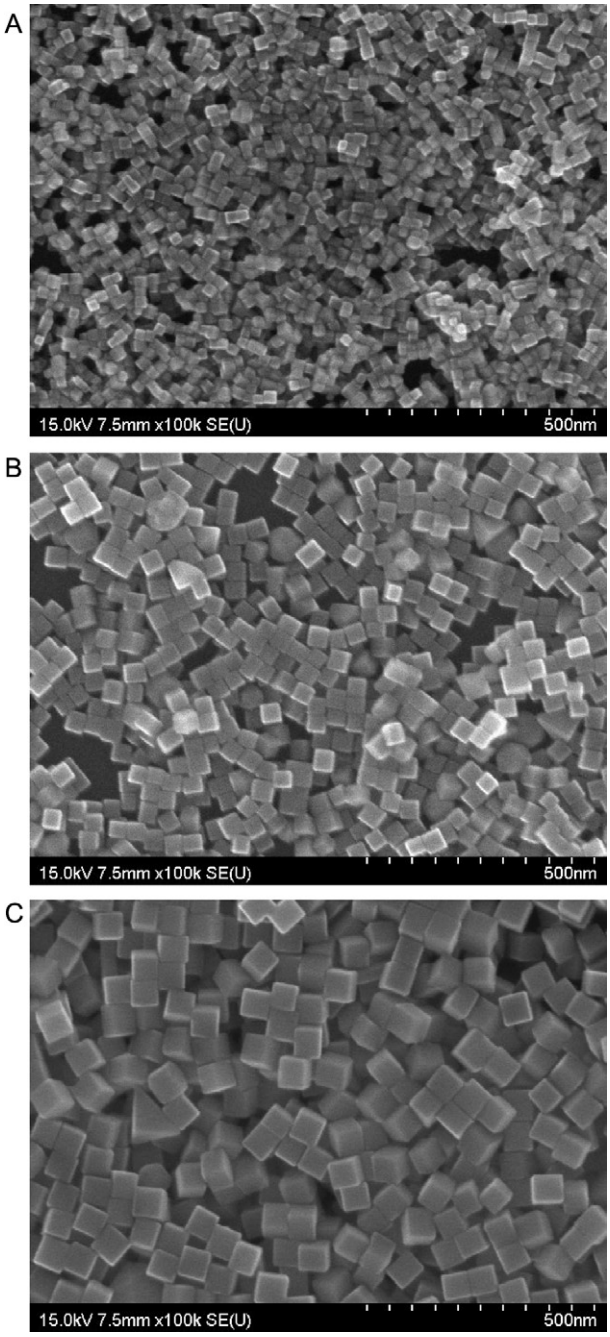

Fig. 3. FE-SEM images of Pd nanocubes: (A) 27 nm nanocubes; (B) 48 nm nanocubes; (C) 63 nm nanocubes.

noted that the area of the hydrogen adsorption/desorption region increases from the 48 nm Pd nanocube to the 27 nm Pd nanocube. The increased area of H_2 reactions indicates a stronger interaction between hydrogen and the Pd nanocubes with a decrease in particle size in the 0.5 M $H_2SO_{4(aq)}$ electrolyte. Compared with CV curves of bulk Pd(1 0 0) planes [28], a more symmetric and well-defined hydrogen adsorption/desorption region was obtained for the 48 nm Pd nanocubes. This indicates that the electrochemical mechanism may be different for bulk and nanoscale catalysts. Furthermore, for a fair comparison, Pd nanoparticles (9 ± 2.1 nm) and Pt nanoparticles (45 ± 7.7 nm) were prepared and their images were obtained using TEM, as shown in Fig. 7A and B, respectively. Fig. 7C reveals the XRD patterns of Pd and Pt nanoparticles. The diffraction peaks for Pd nanoparticles located at 40.56°, 47.04°,

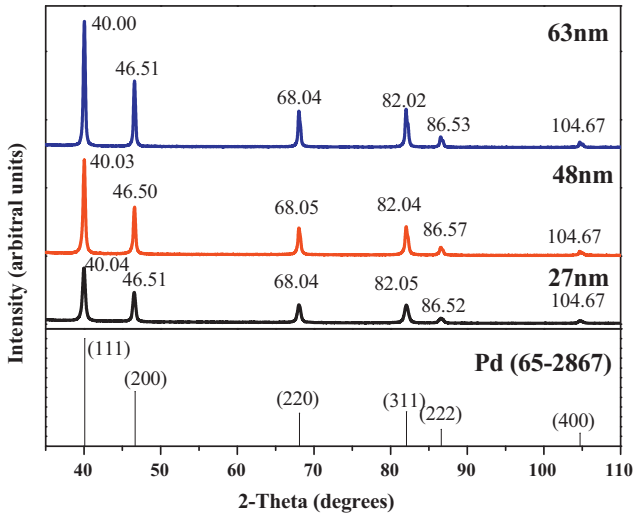

Fig. 4. XRD patterns of the prepared Pd nanocubes.

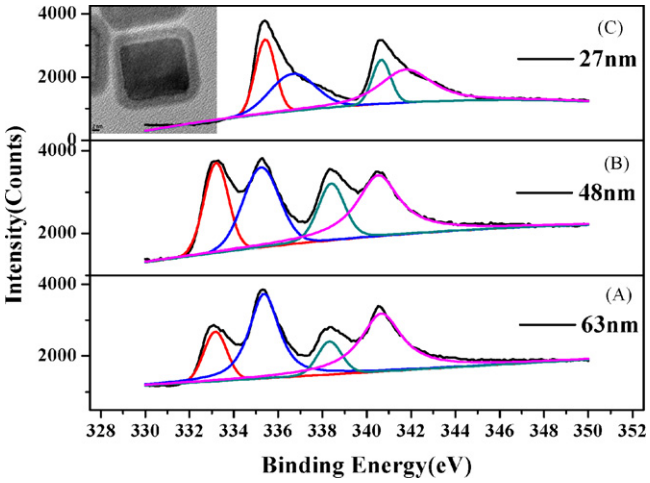

Fig. 5. XPS spectra of the prepared cubic Pd powders. (Inset: HR-TEM image of 27 nm Pd nanocubes.).

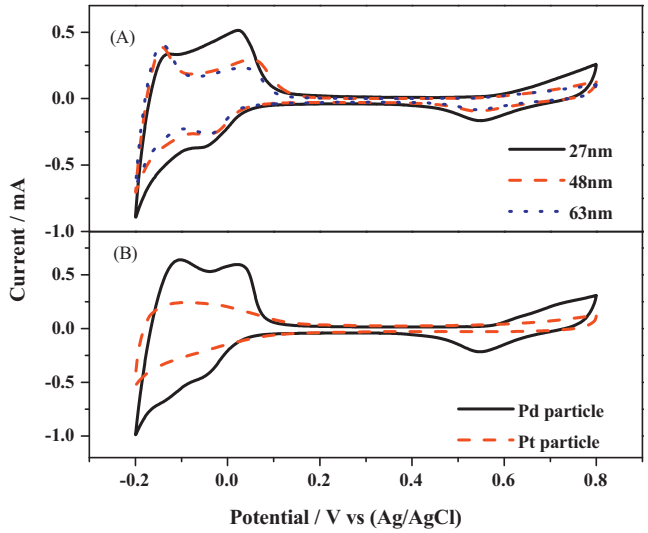

Fig. 6. CV diagrams of the prepared Pd nanocubes, Pt nanoparticles, and Pd nanoparticles in N_2-saturated 1 M $H_2SO_{4(aq)}$ solution. Scan rate: 50 mV s^{-1}. Electrolyte temperature: 25 °C.

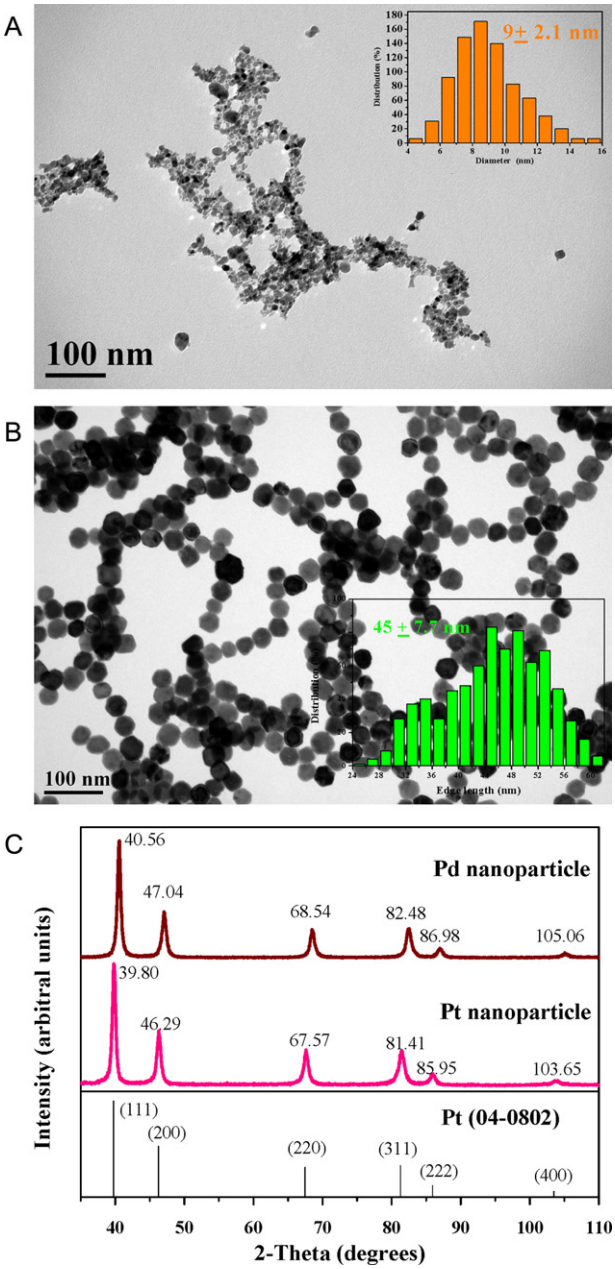

Fig. 7. TEM images and XRD patterns of the Pd and Pt nanoparticles compared to nanocubes: (A) TEM image of Pd nanoparticles; (B) TEM image of Pt nanoparticles; (C) XRD patterns. (The insets in (A) and (B): diameter statistic plot.)

68.54°, 82.48°, 86.98° and 105.06°, similar to standard Pd spectrum in Fig. 4. Also, the peaks of Pt nanoparticles located at 39.80°, 46.29°, 67.57°, 81.41°, 85.95°, and 103.65°, which were consistent with standard fcc spectrum of Pt (JCPDS 04-0802). The composition of the prepared nanoparticles for catalytic comparison was thus identified. Then, based on the same catalyst loading, the electrochemical CV responses of these Pd and Pt nanoparticles relative to those of the Pd nanocubes were measured; the responses are shown in Fig. 6B. It should be noted that the order 9 nm Pd nanoparticle ≧ 27 nm Pd nanocube > 48 nm Pd nanocube > 63 nm Pd nanocube was obtained for the area of the hydrogen desorption region (H_{der}). The H_{der} areas of the 27 nm, 48 nm, and 63 nm Pd nanocubes were 1.273, 0.76, and 0.60 mC, respectively. For the Pd nanoparticles, which are typically dominated by (1 1 1) planes, a clear region of hydrogen adsortpion/desorptionsimilar to the H_{der} of the 27 nm nanocubes surrounded by {1 0 0} facets was observed.

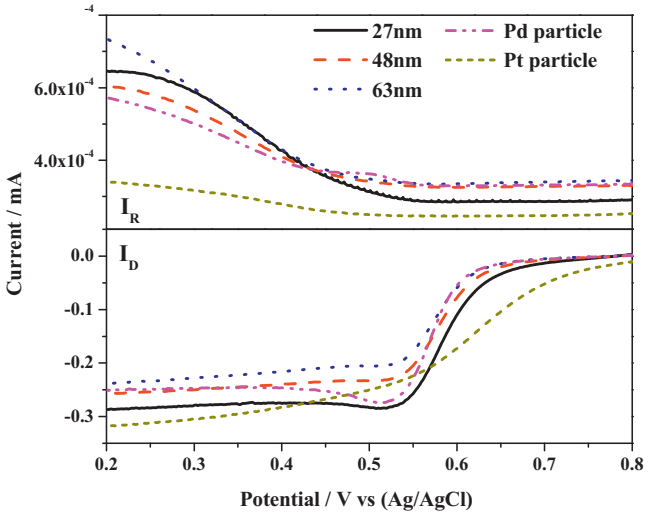

Fig. 8. LSV curves obtained using RRDE measurements for Pd nanocubes, Pt nanoparticles, and Pd nanoparticles in O_2-saturated 1 M $H_2SO_{4(aq)}$ solution. Scan rate: 10 mV s^{-1}. Electrode rotating speed: 500 rpm. Electrolyte temperature: 25 °C.

The H_{der} area of the 27 nm Pd nanocube was approximate to that of the Pd nanoparticle, 1.277 mC. This indicates that the interaction of hydrogen with the 27 nm Pd nanocubes is almost equal to that with 9 nm Pd nanoparticles.

Fig. 8 show LSV curves for the O_2 reduction catalyzed by the various Pd nanocubes, Pd nanoparticles, and Pt nanoparticles dispersed on the 0.196 cm^2 disk electrode; H_2O_2 production was measured in situ by the Pt ring electrode at 1.2 V (vs. Ag/AgCl) in the 0.5 M $H_2SO_{4(aq)}$ electrolyte. The rotating speed of the RRDE electrode was set to 1600 rpm. Here, in order to prevent interference from the PdO produced on the 27 nm Pd nanocubes, the nanocatalyst was dispersed in H_2O and not as a dry powder and was coated on the GC disk electrode for the RRDE analyses. Therefore, the contribution from the reduction of PdO for the 27 nm Pd nanocubes is not observed on the LSV curve. A long electron-transfer (ET) period between 0.8 and 0.675 V, mixed control of ET-diffusion from 0.675 to 0.54 V, and saturated diffusion control below 0.54 V were observed. Similar catalytic potentials were observed for the 48 nm and 63 nm Pd nanocubes and the Pd nanoparticles. In contrast, the Pt nanoparticles showed a higher current in the ET region and reached an early mixed-control ORR catalysis without methanol. Moreover, to precisely compare the specific activities of the Pd nanocubes, Pd nanoparticles, and Pt nanoparticles toward ORR in a 0.5 M $H_2SO_{4(aq)}$ electrolyte, an estimation of the mass-transfer-corrected kinetic current densities (j_k) is necessary. According to a detailed study on comparable Pt catalysts for the ORR involving a thin-film rotating disk experiment, j_k can be calculated by [29]

$$j_k = \frac{(i_d \times i/i_d - i)}{r_f \times A_{geo}} = \frac{(i_d \times i/i_d - i)}{RSA} = \frac{i_k}{RSA}, \quad (1)$$

Here, i_d is the diffusion limiting current at 0.5 V (vs. Ag/AgCl at 25 °C), A_{geo} is the geometric surface area (0.196 cm^2), r_f is the roughness factor, i_k is the kinetic current and RSA is the real surface area. For Pd nanocubes and Pd nanoparticles, RSA can be obtained by intergrating the charge of PdO reduction around 0.55 V (Fig. 6) over 405 μC cm^{-2}, which is a theoretical value for the reduction charges of palladium oxide [30]. The RSA of Pt nanoparticles can be calculated considering the H_{der} charge (Fig. 6B) over 210 μC cm^{-2} [29]. Mass-corrected Tafel plots in terms of j_k for the different catalysts are shown in Fig. 9; the plots are obtained from the disk current shown in Fig. 8. The Tafel slopes for the various Pd nanocubes and Pd nanoparticles were equal to −60 mV dec^{-1} at low current densities. At higher current densities below approximately 0.7 V,

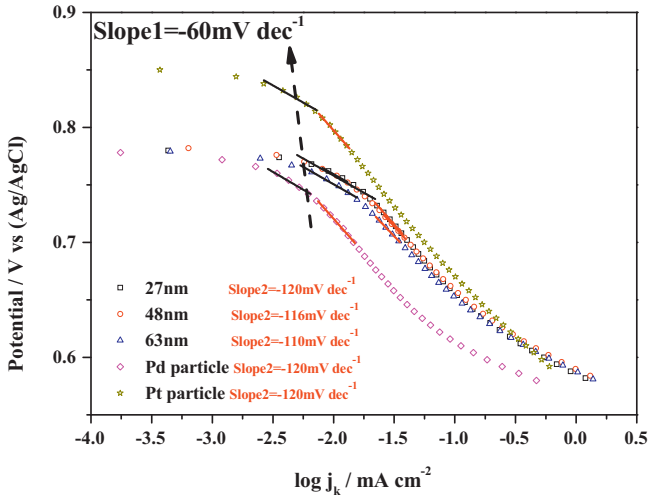

Fig. 9. Mass-transfer corrected Tafel plots of the ORRs on the Pd nanocubes, Pt nanoparticles, and Pd nanoparticles corresponding to specific activity in a free methanol electrolyte.

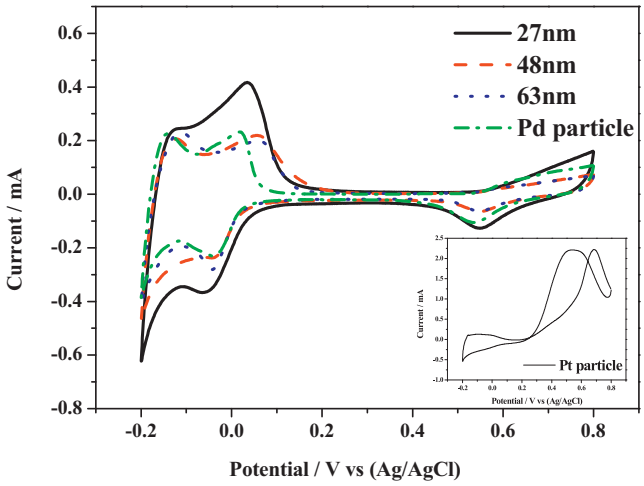

Fig. 10. CV curves of different Pd nanocubes, and Pd nanoparticles in O_2-saturated 0.5 M methanol/1 M $H_2SO_{4(aq)}$ solution. (Inset: CV curve of Pt nanoparticles.)

the Tafel slopes of the 27 nm, 48 nm, and 63 nm Pd nanocubes were −120 mV dec^{-1}, −116 mV dec^{-1}, and −110 mV dec^{-1}, respectively, while that of the Pd nanoparticles was −120 mV dec^{-1}. Similar results were found for nanoscale Pd films [31], bulk Pd films [32], and Pt nanoparticles in this study. For the Pt nanoparticles, the Tafel slope at low current densities was −60 mV dec^{-1} above 0.8 V. As the current density increased, the Tafel slope changed to −120 mV dec^{-1}. The change in the slope for Pt catalysts has been attributed to the change from Temkin to Langmuir conditions for the adsorption of oxygen intermediates, and the transfer of the first electron to O_2 is the rate determining step in the low and high current regions [31,32]. Evidently, a similar coverage change of the reaction intermediate on Pd nanocubes also caused a change in the Tafel slopes of the two regions. Furthermore, a comparison of the specific activity, depicted in Fig. 9, showed the order 48 nm Pd nanocubes > 27 nm Pd nanocubes > 63 nm Pd nanocubes ≫ Pd nanoparticles. The nanocubes enclosed by {1 0 0} facets showed a higher activity than Pd nanoparticles, which is a typical fcc catalyst. Recently, Kondo et al. reported that the specific activity of a bulk electrode of single crystalline Pd(1 0 0) toward acidic ORRs was nearly 14 times as high as that of Pd(1 1 1) [20]. In this study, at 0.65 V (vs. Ag/AgCl), the j_ks of 27 nm, 48 nm, and 63 nm nanocubes were 11.51×10^{-2} mA cm^{-2}, 12.33×10^{-2} mA cm^{-2}, 10.61×10^{-2} mA cm^{-2}, respectively. The j_k by 48 nm Pd nanocube was approximately 3.33 times greater than 3.70×10^{-2} mA cm^{-2}, the j_k of 9 nm Pd nanoparticles. This comparison for the higher activity by the 48 nm Pd nanocubes than the Pd nanoparticles is confirmed by the similar ORRs results using Pd nanocubes and Pd nanoparticles in a 0.5 M H_2SO_4 electrolyte [33] and in a 0.1 M $HClO_4$ [34]. Additionally, note that the kinetic current (i_k) for the LSV curve of ORR can be found a key factor to influence specific activity. The i_k by 63 nm Pd nancube at −0.65 V (vs. Ag/AgCl) was1.5×10^{-2} mA and smaller than 2.2×10^{-2} mA, the i_k by 48 nm nanocube. Obviously, the small i_k by larger nanocube can lead to decrease the j_k and further slow kinetic.

Furthermore, the j_k value of 12.33×10^{-2} mA cm^{-2} for the 48 nm Pd nanocubes was smaller than 13.28×10^{-2} mA cm^{-2}, the j_k of the Pt nanoparticles. Climent et al. [35] found that the inhibition effect, which reduces ORR activity, was greater in Pd catalysts than in Pt(1 1 1) catalysts due to SO_4^{2-} adsorption in 0.5 M $H_2SO_{4(aq)}$ solution. In this study, in the 0.5 M $H_2SO_{4(aq)}$ electrolyte, the dissociated concentration of sulfate ions is likely to be the same with the previous work [35]. The decrease in j_k could be a result of the similar inhibition effect of the sulfate ions. A similar result was found for the 27 nm Pd nanocube, which showed a smaller j_k than 48 nm Pd nanocubes. Additionally, according to these comparisons, Pt nanoparticles are still a better catalyst in fuel cells in the absence of methanol crossover.

In an alcohol fuel cell, the presence of alcohol can force cathodic Pt catalysts to undergo the oxidation reaction of methanol, leading to a considerable loss of ORR activity. This was confirmed by the CV curve of the prepared Pt nanoparticles in the 0.5 M CH_3OH/0.5 M $H_2SO_{4(aq)}$ electrolyte, as shown in the inset of Fig. 10. Additionally, as depicted in the CV curves in Fig. 10, the Pd nanocubes and Pd nanoparticles were all inactive toward methanol oxidation in the 0.5 M $H_2SO_{4(aq)}$ electrolyte with 0.5 M CH_3OH. Here, based on Fig. 10, the RSA values for the 27 nm, 48 nm, and 63 nm Pd nanocubes were 0.21 cm^2, 0.1 cm^2, and 0.089 cm^2, respectively. The RSA of Pd nanoparticles was 0.192 cm^2. Additioanlly, according to the CV curves of Fig. 6 measured in the electrolyte without methanol, the RSAs for the 27 nm, 48 nm, and 63 nm Pd nanocubes and for the Pd nanoparticles were 0.33 cm^2, 0.18 cm^2, 0.145 cm^2, and 0.406 cm^2, respectively. The measured RSAs without or with methanol were plotted in Fig. 11. As shown in Fig. 11, compared to the RSA without methanol, the decreases in the RSA of the O_2 adsorption for the Pd nanocubes and nanoparticle in the electrolyte with methanol were found. Particularly, the most

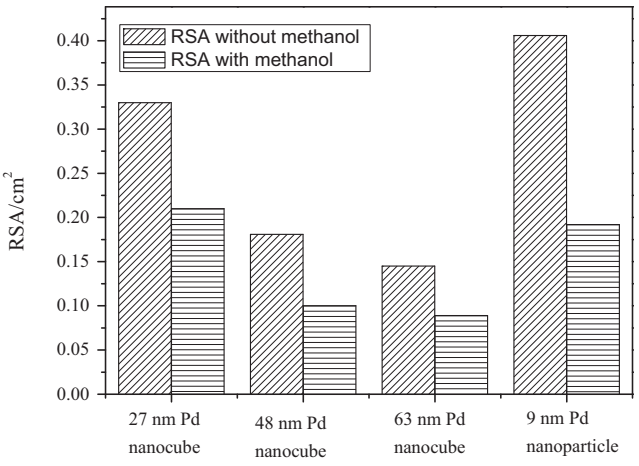

Fig. 11. Comparative bar plots of summarized real surface area without/with methanol derived from Figs. 6 and 10.

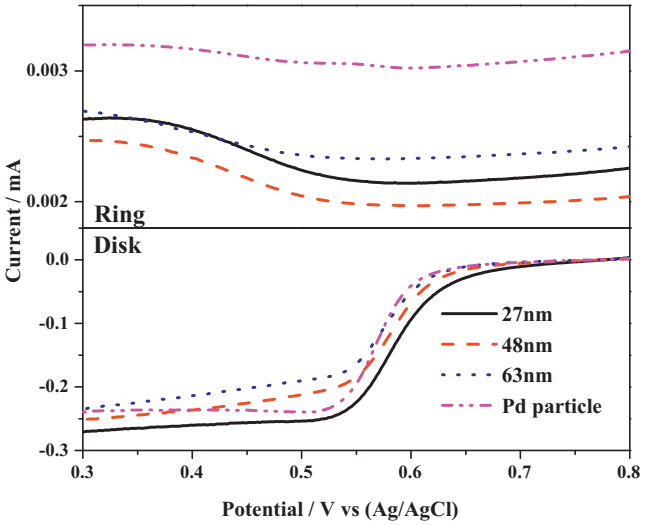

Fig. 12. LSV curves obtained using RRDE measurements for Pd nanocubes, Pt nanoparticles, and Pd nanoparticles in O_2-saturated 0.5 M methanol/1 M $H_2SO_{4(aq)}$ solution. Scan rate: 10 mV s^{-1}. Electrode rotating speed: 500 rpm. Electrolyte temperature: 25 °C.

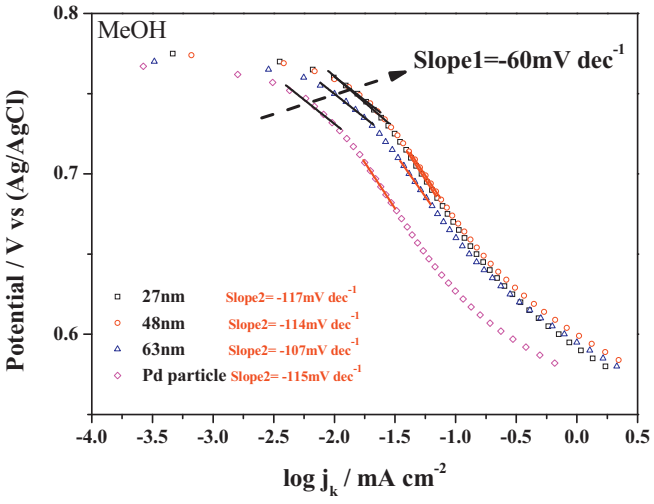

Fig. 13. Mass-transfer corrected Tafel plots of the ORRs on the Pd nanocubes and Pd nanoparticles corresponding to specific activity in a methanol electrolyte.

significant decrease happened on small Pd nanoparticles. This could be resulted from the blockage of the methanol on the surface of Pd catalysts.

Furthermore, the methanol-tolerant properties of Pd nanocubes and Pd nanoparticles toward ORR electrocatalysis were studied by RRDE experiments. Fig. 12 shows polarization RRDE curves for the O_2 reduction catalyzed by the Pd nanoparticles and the prepared Pd nanocubes dispersed on the GCE disk electrode; the H_2O_2 production was determined by in situ measurements using a Pt ring electrode at 1.2 V (vs. Ag/AgCl) in the 0.5 M CH_3OH/0.5 M $H_2SO_{4(aq)}$ electrolyte. As revealed in Fig. 12, all the prepared Pd nanocubes showed high tolerance to the presence of methanol and were active toward ORRs while the potential was scanned. In comparison with the polarization curves shown in Fig. 8, the i_d values measured in Fig. 12 were slightly lower and the corresponding I_r values were much higher indicating that blockage by methanol decreased the reduction power toward O_2 and increased the amount of H_2O_2. For Pd nanoparticles, a reduced current as well as an increased overpotential was observed. The onset potential for ORR shifted from 0.78 V (Fig. 8) to 0.68 V (Fig. 12), indicating the blockage effect of methanol. According to Fig. 12 and the estimated RSA with methanol, the Tafel curves in term of j_k using Eq. (1) for the interference of methanol was studied and shown in Fig. 13. As making a contrast with the Tafel curves without methanol (Fig. 9), the similar adsorption behavior of oxygen even the present of methanol on Pd catalysts was observed. The order of specific activity of 48 nm Pd nanocube > 27 nm Pd nanocube > 63 nm Pd nanocube > 9 nm Pd nanoparticle was obtained. It is worth noting that a slightly higher j_k value was obtained for the Pd nanocube and nanoparticle ORR kinetics with methanol; for 27 nm nanocube, the j_k value increased from 11.51×10^{-2} mA cm^{-2} without methanol to 14.88×10^{-2} mA cm^{-2} with methanol (at 0.65 V). For the 48 nm Pd nanocube, j_k increased from 12.32×10^{-2} mA cm^{-2} to 16.55×10^{-2} mA cm^{-2},while for the 63 nm Pd nanocube, j_k increased from 10.6×10^{-2} mA cm^{-2} to 12.97×10^{-2} mA cm^{-2}, which indicates that there is increased interference from methanol blockage and decreased RSA for oxygen on the Pd nanocube. The increase of approximately 1.96×10^{-2}, from a j_k of 3.7×10^{-2} mA cm^{-2} to 5.6×10^{-2} mA cm^{-2}, for the Pd nanoparticles showed that they have a higher sensitivity toward methanol than Pd nanocubes have. Additionally, {1 0 0} facets of larger Pd nanocubes can enhance plausibly activity in comparison with small Pd nanoparticle, which dominated by (1 1 1) plane shown in Fig. 7C. Based on the above analyses, despite working in the methanol-tolerant solution, the specific activity of the prepared 48 nm Pd nanocube is approximately 2.92 times greater than that of Pd nanoparticles and still exhibited high electroactivity toward the ORR.

4. Conclusion

New methanol-tolerant catalysts in the form of 27 nm, 48 nm, and 63 nm Pd nanocubes enclosed by {1 0 0} facets were successfully used for oxygen electroreduction reactions in 0.5 M $H_2SO_{4(aq)}$ electrolyte. According to RRDE data and mass-transfer Tafel plots, in terms of the kinetic current density, the specific activity order was found to be 48 nm Pd nanocubes > 27 nm Pd nanocubes > 63 nm Pd nanocubes > Pd nanoparticles.

Acknowledgment

The authors would like to thank the National Science Council of the Republic of China, Taiwan, for financially supporting this research under Contract No. NSC 98-2221-E-151-033-MY2 and NSC 100-2221-E-151-044.

References

[1] J.Y. Chen, B. Lim, E.P. Lee, Y.N. Xia, Nano Today 4 (2009) 81.
[2] Y.H. Bing, H.S. Liu, L. Zhang, D. Ghosh, J.J. Zhang, Chem. Soc. Rev. 39 (2010) 2184.
[3] C. Wang, H. Daimon, T. Onodera, T. Koda, S.H. Sun, Angew. Chem. Int. Ed. 47 (2008) 3588.
[4] Q.A. Wang, B.Y. Geng, B. Tao, J. Power Sources 196 (2011) 191.
[5] J. Hernandez, J. Solla-Gullon, E. Herrero, A. Aldaz, J.M. Feliu, J. Phys. Chem. C 111 (2007) 14078.
[6] N.M. Markovic, R.R. Adzic, V.B. Vesovic, J. Electroanal. Chem. 165 (1984) 121.
[7] Z.L. Wang, J. Phys. Chem. B 104 (2000) 1153.
[8] E. Antolini, Energy Environ. Sci. 2 (2009) 915.
[9] S.B. Yin, M. Cai, C.X. Wang, P.K. Shen, Energy Environ. Sci. 4 (2011) 558.
[10] X.W. Li, Q.H. Huang, Z.Q. Zou, B.J. Xia, H. Yang, Electrochim. Acta 53 (2008) 6662.
[11] C.L. Lin, C.M. Sanchez-Sanchez, A.J. Bard, Electrochem. Solid State Lett. 11 (2008) B136.
[12] D.L. Wang, H.L. Xin, Y.C. Yu, H.S. Wang, E. Rus, D.A. Muller, H.D. Abruna, J. Am. Chem. Soc. 132 (2010) 17664.
[13] K. Lee, O. Savadogo, A. Ishihara, S. Mitsushima, N. Kamiya, K. Ota, J. Electrochem. Soc. 153 (2006) A20.
[14] A. Sarkar, A.V. Murugan, A. Manthiram, J. Mater. Chem. 19 (2009) 159.
[15] T. Lopes, E. Antolini, E.R. Gonzalez, Int. J. Hydrogen Energy 33 (2008) 5563.
[16] W.M. Wang, Q.H. Huang, J.Y. Liu, Z.Q. Zou, Z.L. Li, H. Yang, Electrochem. Commun. 10 (2008) 1396.

[17] W.M. Wang, Q.H. Huang, J.Y. Liu, Z.Q. Zou, M.Y. Zhao, W. Vogel, H. Yang, J. Catal. 266 (2009) 156.
[18] C.L. Lee, H.P. Chiou, K.C. Chang, C.H. Huang, Int. J. Hydrogen Energy 36 (2011) 2759–2764.
[19] C.L. Lee, H.P. Chiou, S.C. Wu, C.C. Wu, Electrochim. Acta 56 (2011) 687.
[20] S. Kondo, M. Nakamura, N. Maki, N. Hoshi, J. Phys. Chem. C 113 (2009) 12625.
[21] W.X. Niu, Z.Y. Li, L.H. Shi, X.Q. Liu, H.J. Li, S. Han, J. Chen, G.B. Xu, Cryst. Growth Des. 8 (2008) 4440.
[22] V.L. Nguyen, D.C. Nguyen, T. Hayakawa, H. Hirata, G. Lakshminarayana, M. Nogami, Nanotechnology 21 (2010) 035605.
[23] J. Zhang, H.Z. Yang, K.K. Yang, J. Fang, S.Z. Zou, Z.P. Luo, H. Wang, I.T. Bae, D.Y. Jung, Adv. Funct. Mater. 20 (2010) 3727–3733.
[24] D.R. Lide, CRC Handbook of Chemistry and Physics, CRC Press, London, 2004–2005.
[25] M.S. Bakshi, J. Phys. Chem. C 113 (2009) 10921.
[26] K.S. Kim, A.F. Gossmann, N. Winograd, Anal. Chem. 46 (1974) 197.
[27] Q. Yuan, Z.Y. Zhou, J. Zhuang, X. Wang, Chem. Commun. 46 (2010) 1491.
[28] N. Hoshi, M. Nakamura, S. Kondo, Electrochem. Commun. 11 (2009) 2282.
[29] K.J.J. Mayrhofer, D. Strmcnik, B.B. Blizanac, V. Stamenkovic, M. Arenz, N.M. Markovic, Electrochim. Acta 53 (2008) 3181.
[30] T. Chierchie, C. Mayer, J. Electroanal. Chem. 135 (1982) 211.
[31] H. Erikson, A. Kasikov, C. Johans, K. Kontturi, K. Tammeveski, A. Sarapuu, J. Electroanal. Chem. 652 (2011) 1.
[32] D.B. Sepa, M.V. Vojnovic, L.M. Vracar, A. Damjanovic, Electrochim. Acta 32 (1987) 129.
[33] H. Erikson, A. Sarapuu, K. Tammeveski, J. Solla-Gullon, J.M. Feliu, Electrochem. Commun. 13 (2011) 734.
[34] M. Shao, T. Yu, J.H. Odell, M. Jin, Y.N. Xia, Chem. Commun. 47 (2011) 6566.
[35] V. Climent, N.M. Markovic, P.N. Ross, J. Phys. Chem. B 104 (2000) 3116.